Research Article | Vol. 27, No. 4 | 18 Feb 2019 | OPTICS EXPRESS 5238
Optics EXPRESS

Combining average molecular tilt and flicker for management of depolarized light in parallel-aligned liquid crystal devices for broadband and wide-angle illumination

ANDRÉS MÁRQUEZ,[1,2,*] FRANCISCO J. MARTÍNEZ-GUARDIOLA,[1,2] JORGE FRANCÉS,[1,2] SERGI GALLEGO,[1,2] INMACULADA PASCUAL,[1,2] AND AUGUSTO BELÉNDEZ[1,2]

[1]*Dept. de Física, Ing. de Sistemas y Teoría de la Señal, U. de Alicante, Ap. 99, E-03080, Alicante, Spain*
[2]*I.U. Física Aplicada a las Ciencias y las Tecnologías U. de Alicante, Ap. 99, E-03080, Alicante, Spain*
[3]*Dept. de Óptica, Farmacología y Anatomía, Universidad de Alicante, Ap. 99, E-03080, Alicante, Spain*
[*]*andres.marquez@ua.es*

Abstract: We demonstrate a complete semiphysical and analytical model describing the angular and wavelength dependencies not only of retardance, but also its flicker, in parallel aligned liquid crystal (PA-LC) devices. It relies on the fitting of the molecules' equivalent tilt angle as a function of applied voltage. The wide range of calculations it offers without requiring extensive characterization makes the model unique. We focus on PA-LCoS application as a polarization state generator across the visible spectrum and for a wide range of incidence angles. This approach offers novel capabilities for managing arbitrary states of both full and partial polarization. To highlight the richness of situations with PA-LCoS devices, we provide results for two different digital addressing sequences producing different levels of flicker.

1. Introduction

Liquid crystal on silicon (LCoS) microdisplays have become one of the main technologies for a very wide range of spatial light modulation applications [1–3]. Among them, parallel-aligned LCoS (PA-LCoS) are especially appealing since they enable phase-only operation without amplitude coupling [4,5]. PA-LCoS can be found in many optics and photonics applications such as in diffractive optics [6], optical storage [7,8], optical metrology [9], reconfigurable interconnects [10,11], wavefront sensing of structured light beams [12], holographic optical traps [13], or quantum optical computing [14]. In recent years, a wide interest has arisen dealing with the generation and detection of unconventional polarization structured wavefronts [15,16] in which PA-LCoS devices play a central role [17,18].

Something attractive about PA-LCoS is that they can be easily modelled as a variable linear retarder. Therefore, they can be characterized by their linear retardance as a function of the applied voltage. However, the existence of flicker in many of these devices, especially the ones digitally addressed [19–22], has resulted in the proposal of more complete models and characterization methods. In these methods the flicker in the linear retardance is also measured, such as in the time-averaged Stokes polarimetric technique [23], the one proposed by Ramírez et al. [24] or other techniques based on interferometric measurements [25] using high-speed cameras [26]. All these models and characterization methods consider the PA-LCoS as a polarization-changing device without introducing parameters related with its internal properties. Therefore, these reverse-engineering characterization methods are based on "black-box" models.

Physical models, i.e. based on the actual internal properties, are more precise. However, they tend to be more sophisticated including many material and device parameters, whose

#351292 https://doi.org/10.1364/OE.27.005238
Journal © 2019 Received 9 Nov 2018; revised 17 Jan 2019; accepted 18 Jan 2019; published 12 Feb 2019

Optics EXPRESS

values need to be known beforehand. This is the case for LC devices where the different parameters characterizing the LC material and the LC cell must be known [2,3]. Additionally, rigorous physical modelling of a LC device requires numerical evaluation both to calculate the LC director orientation across the LC cell [2,3], and then to calculate the propagation of the electromagnetic field across the device [27–30]. However, availability of analytical expressions would facilitate easier access to physical insight into the performance of the device. As a result, we proposed and demonstrated a simplified physical model for PA-LC devices [31], where only the most relevant internal parameters remained such as the equivalent LC molecular tilt. In the following, we will call it semiphysical model since it is a simplified version of the rigorous approach. This semiphysical model provides the voltage dependent retardance for a very wide range of incidence angles (from 0 to 45°) and any wavelength in the visible spectrum. We have further demonstrated that the fitted values obtained for two of the three parameters in the model are equal to the actual values. Thus, the model shows not only predictive capability but it also enables to probe into the internal properties of PA-LCoS devices [32,33].

To calibrate the parameters in the semiphysical model we need to measure the retardance at certain configurations [31]. When using the time-averaged Stokes polarimetric technique [23] we measure both the average retardance and its flicker amplitude. In previous works, we only considered the average retardance value measured with this technique, which enables to obtain the equivalent tilt angle of the LC-director across the cell as a function of the applied voltage. Then, a natural step forward is to analyse the flicker amplitude measurements. We want to learn to which extent the semiphysical model is able to predict the magnitude of this flicker at other wavelengths and incidence angles different from the measured ones. This is interesting so that we can further calculate if the degradation effects introduced by the phase flicker are within the tolerance limits for the application at hand. This tolerance evaluation was done for example by Lizana et al. [34] and by Martínez et al. [35] in the application to diffractive optics. We also believe that in order to get further insight into the physics in the device, it is very appealing connecting the flicker in the retardance with instabilities in the tilt angle for the LC director. This connection might provide information about the dynamics in the LC layer and might also be an alternative tool to estimate other physical parameters of the LC material in the device. Another interesting application is the evaluation and management of partially depolarized light, as we will show in this paper, where we can actually predict the degree of polarization across the visible spectrum, for a wide range of incidence angles and for any input state of polarization (SOP). This might be a useful tool to generate unconventional polarized beams with a certain amount of depolarization.

In this work, we both use experimental average retardance and flicker measurements to analyse the predictive capabilities of the semiphysical model. We do it for two different digital addressing sequences with different levels of flicker. In our model, this flicker in the retardance is due to instabilities in the tilt angle orientation, thus connecting with the dynamics of the LC material in the device. We are interested in showing the relevance and versatility of our approach to predict and control the polarization states and the depolarization generated by the PA-LCoS devices.

2. Methods and experimental implementation

The specific PA-LC device considered in this work is a commercially available PA-LCoS microdisplay, model PLUTO distributed by the company HOLOEYE. It is a nematic liquid crystal filled, with 1920x1080 pixels and 0.7” diagonal, whose backplane is digitally addressed [19,22]. In the digital drive scheme a pulse width modulation (PWM) is used. This means a high-frequency series of binary voltage pulses, referred to as addressing sequence, leads to the desired gray-level representation. Due to the limited viscosity of the liquid crystal material the base addressing frequency cannot be resolved [19]: the nematic LC responds to the root-mean square (RMS) value of the driving voltage over the characteristic switching

Optics EXPRESS

time of the LC and the residual AC modulation is responsible for the flicker described in digital LCoS devices [22].

Different PWM addressing schemes (digital addressing sequences) can be generated by the driver electronics [19,22]. The time constants of the successive bit-planes in the digital addressing are constant for a number of "equally weighted" bit-planes, and are then reduced by a factor of two for each of the following "binary" bit-planes [19]. We have selected two electrical sequences exhibiting a clearly different scale of fluctuations, whose configuration files are provided with the software. They correspond to the configurations labelled as "18-6 633 2pi linear" and "5-5 633 2pi linear". The first number indicates the quantity of "equally weighted" bit-planes, and the second number the quantity of "binary" bit-planes [19,22]. This means that the sequence 18-6, which has 24 bit planes, is longer than the one corresponding for the sequence 5-5, with ten bit planes. Within a frame period, the shorter sequence will be repeated more times than the longer sequence. In principle the shorter the sequence the smaller the flicker [19,22], since higher modulation rates cannot be followed by the LC material. However, a larger sequence provides a larger number of possible phase levels: $(18 + 1) \times 2^6 = 1216$ for the sequence "18-6" and $(5 + 1) \times 2^5 = 192$ for the sequence "5-5". These sequences are optimized for phase-only operation with a 2π radians linear phase dynamic range for 633 nm at normal incidence. They could be optimized for other wavelengths and applications as shown by Martínez et al. [22].

The time-averaged Stokes polarimetric measurements have been obtained with a Stokes polarimeter, model PAX5710VIS-T distributed by the company THORLABS [23]. The polarimeter averaging time considered, 600 ms, is much larger than actually needed to obtain fully stable and repeatable SOP measurements: time period (frequency) for the fluctuations in our PA-LCoS device is 8.66 ms (120 Hz). Measurements have been taken at various angles of incidence (3°, 23°, 35° and 45°) and for three wavelengths (473, 532 and 633 nm) sampling the visible spectrum. We use the measurements taken at 3° and 35° for calibration, and the measurements at 23° and 45° to assess the predictive capability of the semiphysical model. To obtain the experimental values for the average retardance and for its flicker amplitude, we measured the averaged Stokes vector parameters for an input light beam linearly polarized light at + 45° with respect to the LC director in the LCoS microdisplay, as shown in [23].

3. Results

3.1 Semiphysical model with molecular tilt angle flicker

The proposal of the semiphysical model for PA-LC devices within the context of average retardance values was given by Martínez et al. [31]. For the sake of self-containment of the paper, in this Section we first provide a brief description of this approach. Then we present its extension to the full case where flicker is also considered, so that the semiphysical model potential is fully exploited.

We note that, for average values, in [31] Martínez et al. showed that the agreement with experimental measurements was already verified for a commercial reflective PA-LCoS device. Afterwards, we have further shown [32] that the fitted values obtained for two of the three parameters in the model are equal to the actual values, thus these parameters are physically meaningful: one of these two parameters is the LC molecular equivalent tilt angle versus the applied voltage.

Optics EXPRESS

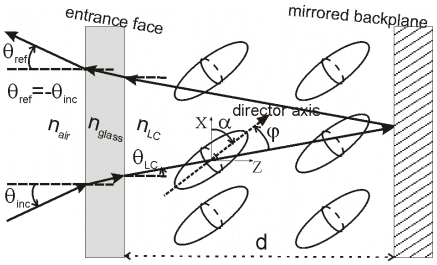

Fig. 1. Diagram for the PA-LC cell considered in the semiphysical model.

In Fig. 1 we show the general diagram considered for a reflective cell with a cell gap d. Incidence plane and LC director are along the XZ plane. LC molecules have their director axis (optical axis) aligned at an angle ϕ with respect to the traversing light beam direction. θ_{LC} is the refraction angle in the LC medium. The director axis tilts an angle α with respect to the entrance face as a function of the applied voltage V. This is the only voltage dependent magnitude, i.e. $\alpha(V)$. At the backplane the light beam is reflected and a second passage is produced across the LC layer whose effect is equivalent to a forward propagation at an angle $-\theta_{inc}$. In the model we define two off-state parameters, combination of the LC indices ordinary and extraordinary, n_o and n_e, together with the cell gap d. They are $OPL = dn_o$ and $OPD = d\Delta n$, which correspond respectively to the magnitudes of the optical path length (OPL) for the ordinary component and the optical path difference (OPD) between extraordinary and ordinary components. Proper derivation leads to the following analytical expression for retardance [31],

$$\Gamma = \frac{2\pi}{\lambda}\frac{OPL}{\cos\theta_{LC}}\left[\frac{1+(OPD/OPL)}{1+(OPD/OPL)\cos^2\phi}-1\right] \tag{1}$$

According to Fig. 1, angle ϕ is given by,

$$\phi(\theta_{inc},V) = \frac{\pi}{2}+\alpha(V)\mp\theta_{LC}(\theta_{inc}) \tag{2}$$

where the minus (plus) sign applies for the forward (backward) passage. The total retardance in the PA-LCoS is given by the addition of the forward and backward retardances. In the case of normal incidence and LC director axis parallel to the entrance face, then Eq. (1) simplifies into the well-known expression $\Gamma = 2\pi d\Delta n/\lambda$.

We note that in our previous works [31,32], as candidate to simplified physical model, we also evaluated the exact expressions for a homogeneous uniaxial anisotropic plate [3,30]. Both models disregard the fact that the tilt angle of the LC director changes across the cell. Our model adds a second approximation, since it does not take into account the double refraction. However, we obtained that both simplified models show the same level of predictive capability, with the benefit that our model produces a much simpler expression and reduces the number of parameters when compared with these exact expressions. Additionally, when fitting the parameters, our model converges to a unique solution, whose values are equal to the real physical values in two of its three parameters [32]: OPD and equivalent molecular tilt angle $\alpha(V)$. This was not the case with the exact expressions.

To obtain the values for the parameters in the model, a reverse-engineering approach is considered: a standard non-linear iterative fitting procedure is applied between the theoretical expression in Eq. (1) and experimental retardance measurements. Off-state measurements,

Optics EXPRESS

LCoS switched-off, are used to obtain OPL and OPD values. Then we proceed with the on-state measurements to obtain the tilt angle $\alpha(V)$ for each applied voltage.

Until now, the semiphysical model has been used only with average retardance values, however there are measurement techniques, such as the time-averaged Stokes polarimetric technique [23], which provide both the average retardance $\overline{\Gamma}$ and its flicker amplitude $\Delta\Gamma$ at each applied voltage. Since the flicker is related with fluctuations in the applied voltage, the OPD and OPL values are unaffected, and all the flicker is due to fluctuations in the molecular tilt angle. To fully exploit the potential of our semiphysical model, what we propose is to define the maximum and the minimum expected retardance values, given respectively as $\Gamma_+ = \overline{\Gamma} + \Delta\Gamma$ and $\Gamma_- = \overline{\Gamma} - \Delta\Gamma$. Using them in the fitting procedure we obtain the tilt angles $\alpha_+(V)$ and $\alpha_-(V)$ associated respectively with the experimental values Γ_+ and Γ_-. Then, the flicker in the tilt angle for the LC molecular director $\Delta\alpha(V)$ is calculated at each applied voltage as the average absolute difference, $\Delta\alpha = |\alpha_+ - \alpha_-|/2$. As a result, with the addition of the flicker in the molecular tilt angle $\Delta\alpha(V)$ the semiphysical model incorporates a fourth parameter of a different nature: this novel parameter provides information about the dynamics of the specific LC compound used in the LC layer, whereas the other three are only related with static properties. This is interesting and may lead to novel applications, however, in the present paper, we focus on the capability of this full version of the semiphysical model for management of light polarization, including the possibility of partially depolarized light.

3.2 Off-state parameters calibration and robustness analysis

Table 1. Values for the retardance in the off-state.

λ	Incidence angle			
	3°	23°	35°	45°
(nm)	(deg)	(deg)	(deg)	(deg)
633	599.5	562.4	538.3	506.5
532	802.8	771.3	718.5	703.2
473	987.0	945.6	900.3	867.1

Table 2. Fitted OPD and OPL obtained using the retardance values in Table 1.

λ (nm)	633	532	473
OPD(μm)	0.5275	0.5937	0.6489
OPL(μm)	2.5761	2.6064	6.8925

In Table 1 we show the off-state retardance measurements, that is, obtained when the PA-LCoS is switched-off. Let us first consider these measurements as if they had no error or uncertainty till the fourth significant digit, so that we can discuss the robustness of the model and characterization approach afterwards. In Table 2 we show the fitted values for OPL and OPD obtained using the off-state measurements in Table 1 at angles of incidence 3° and 35°. A standard non-linear iterative fitting procedure is applied between the theoretical expression in Eq. (1) and the experimental retardance measurements in Table 1. The figure of merit to be minimized combines two squared differences: on one hand between theoretical and experimental retardance values normalized by the experimental value, and on the other hand between the theoretical and experimental ratios of the retardance values at 3° and 35° incidence normalized by the experimental ratio. These two normalized squared differences are added up for the three wavelengths.

In recent works [31–33], we obtained that the semiphysical model proposed is able to provide the values for the parameters OPD and OPL without ambiguities. The resulting values obtained for these two parameters were the same to more than the fourth significant digit independently of the starting values considered for OPD and OPL in the non-linear

Optics EXPRESS

iterative fitting procedure. To stress this convergence property of the model we included the values in Tables 1 and 2 with such a precision.

Now, we want to analyse the robustness of the values for OPD and OPL to the actual uncertainties in the experimental retardances employed in the fitting procedure. In a previous paper [36] we analysed the robustness of the measurements with the average Stokes polarimetric technique when characterizing PA-LCoS microdisplays: these retardance measurements can be associated with a relative uncertainty about 1%. This means that for the retardance measurements in Table 1, they are reliable until the third digit. We have run the fitting procedure to obtain that the relative uncertainty in the resulting OPD and OPL values is also 1%. As a result, in Table 3 we present the OPD and OPL fitted values with their associated absolute uncertainties. Actually, further analysis leads us to conclude that the OPD and OPL relative uncertainties are always equal to the relative uncertainty given by the experimental retardances used in the fitting procedure.

Table 3. Fitted OPD and OPL obtained for the retardance values in Table 1 with 1% uncertainty.

λ (nm)	633	532	473
OPD(μm)	0.528 ± 0.005	0.594 ± 0.006	0.649 ± 0.006
OPL(μm)	2.58 ± 0.03	2.61 ± 0.03	6.89 ± 0.07

3.3 On-state parameters calibration: average tilt angle and flicker amplitude

Once we have the off-state parameters, OPD and OPL, we fix these values in the theoretical expressions for the semiphysical model. Then, we use the on-state average retardance and flicker amplitude values for incidence angles at 3° and 35° as the experimental values for the fitting procedure with the theoretical expressions. From the average retardance fit we obtain the tilt angle as a function of voltage $\alpha(V)$. The same figure of merit function previously explained in the off-state calibration is now used for the on-state fitting procedure, and the optimization is run independently for each of the gray level (equivalent to applied voltage) values. We proceed identically with the maximum $\Gamma_+ = \overline{\Gamma} + \Delta\Gamma$ and the minimum $\Gamma_- = \overline{\Gamma} - \Delta\Gamma$ experimental values to calculate, as earlier explained, the flicker in the tilt angle $\Delta\alpha(V)$.

In Fig. 2 we show the tilt angle $\alpha(V)$ as a function of the gray level addressed with the graphics card, which is related with the applied voltage. We see the resulting values for the two sequence format configurations, 5-5 and 18-6, previously presented. The tilt angle increases monotonically with the gray level, i.e. the applied voltage increases with the gray level. We also note that the curve is highly nonlinear at lower gray levels. The two sequences follow similar but slightly shifted curves with sequence 18-6 producing slightly larger tilt angle values, with maximum values about 50° in both cases. This means that we are still within the range where tilt angle profiles across the cell thickness do not saturate in the cell bulk [33], i.e. the tilt angle is smaller than 90° in the midlayer. This is the situation where the tilt angle can be approximated as a sine-like profile, which is when our model shows the best agreement with experiment [32,33]. At 0 gray level the tilt angle is about 5° and 10° respectively for sequences 5-5 and 18-6, which means that the applied voltage is larger than the threshold value in both sequences and larger for 18-6 than for 5-5.

Optics EXPRESS

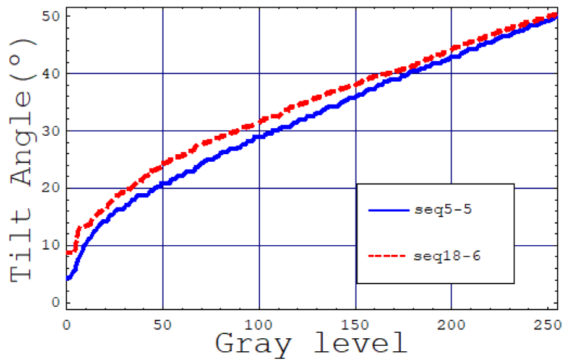

Fig. 2. Tilt angle as a function of gray level obtained for the two sequence formats considered.

The result obtained for the molecular tilt flicker $\Delta\alpha(V)$ for the two sequences is shown in Figs. 3(a) and 3(b), as a function respectively of the gray level and the tilt angle. To pass from Figs. 3(a) to 3(b) we use the mapping between tilt angle versus gray level in Fig. 2. We see that both sequences exhibit a very different behavior for the tilt flicker: for sequence 5-5 is clearly smaller and increases with gray level, whereas for 18-6 it reaches a maximum value about 4.5° and then stays basically constant. We also note in the tilt flicker a series of jumps, which are related with one of the bit planes in the digital sequence changing its state from ON to OFF or viceversa. Due to the nonlinear relation at low gray levels between tilt angle and gray level (see Fig. 2), in Fig. 3(b) the region for low gray levels, corresponding to low tilt angles, becomes stretched. Something important in this analysis is that there is no clear correlation between tilt angle and tilt flicker. Therefore, the tilt flicker is mostly related with the specific pulse structure and amplitude of the applied voltage.

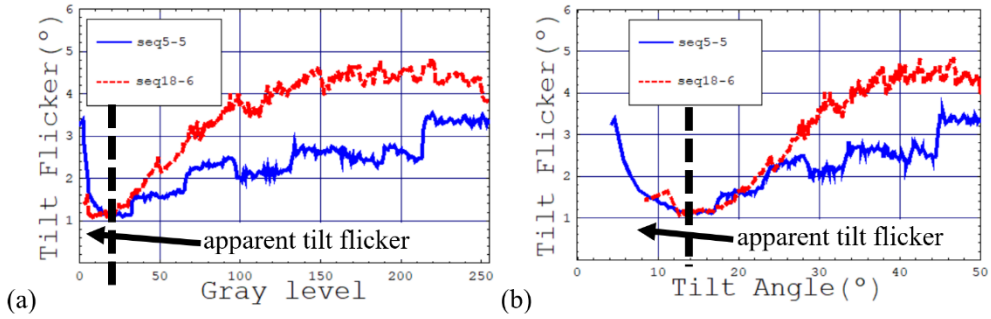

Fig. 3. Tilt flicker for sequence formats 5-5 and 18-6, (a) as a function of gray level, and (b) as a function of average tilt angle.

At very low gray levels (low tilt angles) we see that the tilt flicker increases, especially for sequence 5-5 where it reaches a value larger than 3°. This flicker is not real: we showed in an earlier paper [37] (see Fig. 6 therein) that at 0 gray level there is no flicker for these sequences 5-5 and 18-6. The origin for this "apparent" tilt flicker comes from the kind of experimental measurements that we use to fit the parameters in the model. We consider depolarization measurements provided by the Stokes polarimeter in the time-averaged Stokes polarimetric technique [23]. Even when the PA-LCoS is switched-off we may obtain a certain degree of depolarized light reflected from PA-LC devices [36] due to averaging of spatial inhomogeneities across the aperture of the light wavefront. Possible causes are micrometer scale retardance variations averaged across the pixel, diffraction at the edges of the pixels, disclinations in the LC [38]. We have done the following test to verify the spatial variation of the SOP of light across the aperture of the light wavefront reflected by the LCoS when switched-off. We inserted a diaphragm before the small aperture of the Stokes polarimeter.

Optics EXPRESS

The diaphragm was closed enough so that we could select smaller regions within the aperture of the light wavefront. We obtained that the SOP measured by the polarimeter is different across the aperture of the wavefront. This was much more evident at 45° angle of incidence. We note that this spatial variation of the reflected SOP across the aperture of the light wavefront is wavelength dependent since the LC layer retardance depends strongly on the wavelength. This will produce that the experimental DOP related with this spatial averaging shows wavelength dependency. When incident perpendicular to the device these effects are residual but as the incidence angle increases their importance and its influence on the fitting of the tilt flicker increases as well. In Fig. 3, we have marked with a vertical dashed line the point where the tilt flicker reaches a minimum: at about 20 gray level (14° tilt angle). At lower gray levels (tilt angles), the real tilt flicker actually continues decreasing (in the off-state this would be exactly 0°). Thus, in the plot we have labelled this region as "apparent tilt flicker". We decided to leave these apparent tilt flicker values and use them later when we calculate the state of polarization (SOP) and the degree of polarization (DoP): they are still useful to calculate the amount of depolarized light even though the origin is not tilt flicker.

As we have done at the end of Section 3.2, let us now discuss the robustness of the results obtained for the molecular tilt angle $\alpha(V)$ in Fig. 2 and for the molecular tilt flicker $\Delta\alpha(V)$ in Fig. 3. We do it for sequence 5-5 but the discussion is similar for 18-6. We consider 1% relative uncertainty in the experimental retardance measures used in the fitting procedure. We find that, both for the tilt angle and for the tilt flicker, two scenarios provide the necessary insight in this analysis depending on the deviation considered for the off-state and the on-state experimental retardances. The best scenario happens when the deviation is in the same sense for off-state and on-state retardances, that is, both on-state and off-state retardances increase (or decrease) by 1%: then the tilt angle and the tilt flicker obtained are the same as when no deviation is considered, shown respectively in Figs. 2 and 3. The worst scenario occurs when off-state and on-state deviations are in opposite senses. In this scenario the tilt angle and the tilt flicker deviate the most from the values shown in Figs. 2 and 3. In the case of tilt angle, deviation follows a non-linear fast decrease from ± 4.5° at 0 gray level to 2° at 20 gray level, and then to ± 0.5° at large gray levels, with an average value of ± 1.1° across the 256 gray level range. In the case of the molecular tilt flicker values $\Delta\alpha(V)$, in the worst scenario deviation follows a non-linear fast decrease from ± 1.9° at 0 gray level, to close to 0.1° at gray level 20, and continues decreasing to ± 0.05° at large gray levels, with an average value of ± 0.12° across the 256 gray level range. Thus, both the molecular tilt angle and tilt flicker show a robust behaviour, especially at middle and large gray levels where their relative uncertainty is less than 1%.

3.4 Prediction of retardance and its flicker amplitude

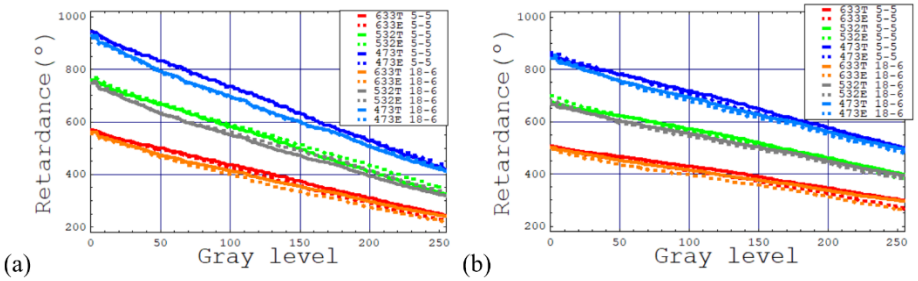

Fig. 4. Experiment (dots) and theoretical prediction with the proposed model (line) for sequence formats 5-5 and 18-6, for the wavelengths 473, 532 and 633 nm and for incidence at: (a) 23°; (b) 45°.

Optics EXPRESS

To show the goodness of the fitted parameter values for OPD, OPL and $\alpha(V)$, next we compare in Fig. 4 the experimental measurements (dots) and the theoretical (line) retardance values calculated with the model, for sequences 5-5 and 18-6 and for the three wavelengths. In Figs. 4(a) and 4(b) we plot the results respectively for incidences at 23° and 45°. We obtain that the agreement is very good, actually with uncertainties smaller than 5% across most of the gray level range, as already demonstrated in previous papers [31–33], both against experimental measurements [31] and against rigorous electromagnetic calculations using Split-Field Finite Difference Time Domain (SF-FDTD) simulations [32,33]. Retardance curves are very similar in all cases for both sequences and very linear with the gray level. The retardance dynamic range decreases as the incidence angle increases, and increases as the wavelength decreases.

In Fig. 5 we compare the measured and the predicted values, calculated using the model, for the retardance flicker amplitude $\Delta\Gamma$ as a function of the applied voltage (gray level): upper and lower row respectively for the sequence 5-5 and 18-6, and for the angles of incidence 23° (left column) and 45° (right column). The agreement for incidence at 23° is very good for both sequences and for the three wavelengths spanning the visible spectrum. For incidence at 45° the agreement is good for middle and large gray levels, but clearly decreases at lower gray levels where we see that the experimental values are much larger than theoretically predicted. As noted earlier when discussing Fig. 3, at lower gray levels the real tilt flicker is actually small and the origin of the large values for the flicker in the fluctuation amplitude is mostly due to other depolarization phenomena different from tilt flicker. We note that, as commented in Section 3.3, the spatial averaging is wavelength dependent. This might help to explain why in Figs. 5(b1) and 5(b2), at low gray levels, the fluctuation amplitudes are very different for the green wavelength when compared with the red and blue wavelengths, which show very large fluctuations and very different from the theoretically predicted values. It is for incidence angles larger than about 30-35° that we obtain this bad agreement at low gray levels between experiment and theory. Therefore, we establish that the model proposed is useful to predict the average retardance in the range between 0 to 45°, and to predict flicker amplitude in the retardance also for a very wide incidence angle range from 0 to 35°.

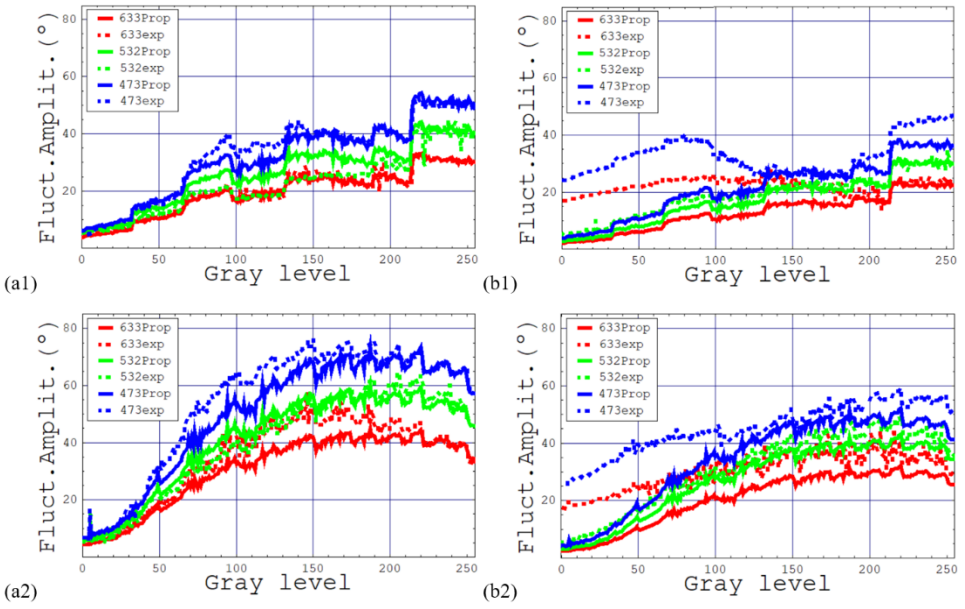

Fig. 5. Experiment (dots) and theoretical prediction with the proposed model (line) for sequence formats 5-5 ((a1) and (b1)) and 18-6 ((a2) and (b2)), for the wavelengths 473, 532 and 633 nm and for incidence at 23° ((a1) and (a2)), and at 45° ((b1) and (b2)).

Optics EXPRESS

3.5. Predictive management of polarized light

Next we analyse the usefulness of the model and its calculated average and flicker retardance values to predict the SOP and DoP for the light reflected by the PA-LCoS device. We use the Mueller-Stokes formalism for polarized light, which includes the possibility of depolarized light. More specifically, we apply the Mueller-Stokes approach we proposed [23] to take into account the existence of flicker in the retardance in PA-LC devices. We will consider that the incident SOP corresponds to right-handed circular light, which generates large modulation in the reflected SOP. We provide measurements and calculations for the three wavelengths, for the two sequences 5-5 and 18-6 and for different angles of incidence.

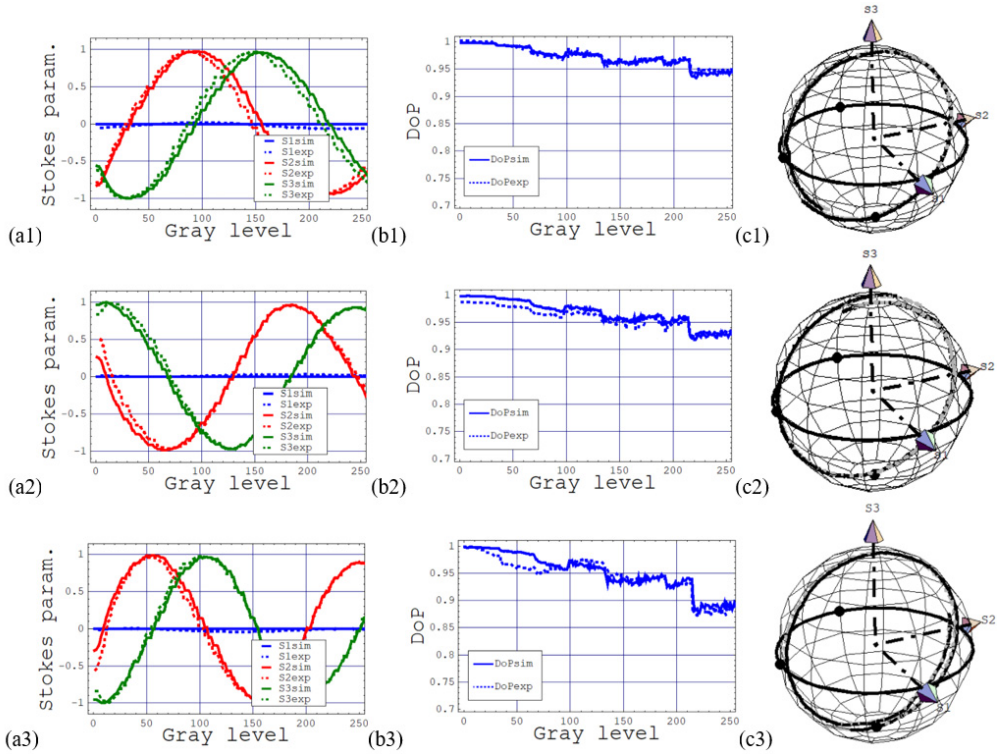

Fig. 6. For sequence format 5-5 and for incident SOP right-handed circular, in plots (a) for the Stokes parameters and in (b) for DoP, experiment (dots) and theoretical prediction with the proposed model (line), and in plots (c) representation on the Poincaré sphere, where the dark line is simulation and gray line is experiment. Top row ((a1), (b1) and (c1)) for 633 nm and incidence at 3°; middle row ((a2), (b2) and (c2)) for 532 nm and incidence at 30°; bottom row ((a3), (b3) and (c3)) for 473 nm and incidence at 30°.

In Fig. 6 we show results for the sequence 5-5, where the first and second columns correspond respectively to the values for the Stokes parameters and for the DoP versus gray level. Dots and lines correspond to experiment and theoretical prediction. In the third column, we show a more global overview of the reflected SOP on the Poincaré sphere, where the dark line is simulation and gray line is experiment. The top row corresponds to illumination with 633 nm and incidence at 3°, middle with 532 nm and incidence at 30° and bottom row with 473 nm and incidence at 30°. We see that agreement between experiment and prediction is very good in all the cases. If we go further from incidence angle 35°, the SOP calculation still agrees well with the experiment. In the case of DoP, the agreement worsens especially at lower gray levels as it also happened in Fig. 5. However, we want to stress that for such a large incidence angle range, from 0° to 35°, and across the whole visible spectrum, the

Optics EXPRESS

semiphysical model is able to provide a good estimation not only for the reflected SOP but also for the DoP independently of the input SOP.

Something that we note from the plots in Fig. 6 is that the interplay between angle of incidence and illumination wavelength enables to control the SOP modulation range. In all three cases in Fig. 6, the SOP travel along the Poincaré sphere stays close to one full meridian. To restrict the modulation range, when using shorter wavelengths, we needed to increase the angle of incidence. This has the additional benefit that for larger angles of incidence the DoP gets closer to one. All this can be properly adjusted using the model. Therefore, our model is highly predictive and is very versatile in such applications as in management and control of polarized light beams.

Next we show in Fig. 7 the same kind of results presented in Fig. 6 but now for sequence 18-6. Once again there is a very good agreement between experiment and theory. The SOP curves are very similar both for the sequence 5-5 and 18-6. However, we see that DoP profiles are very different, being much larger in the case of the sequence 18-6 when compared with sequence 5-5. As in Fig. 6, the plots provided in Fig. 7 are designed so that the SOP travel along the Poincaré sphere stays close to one full meridian.

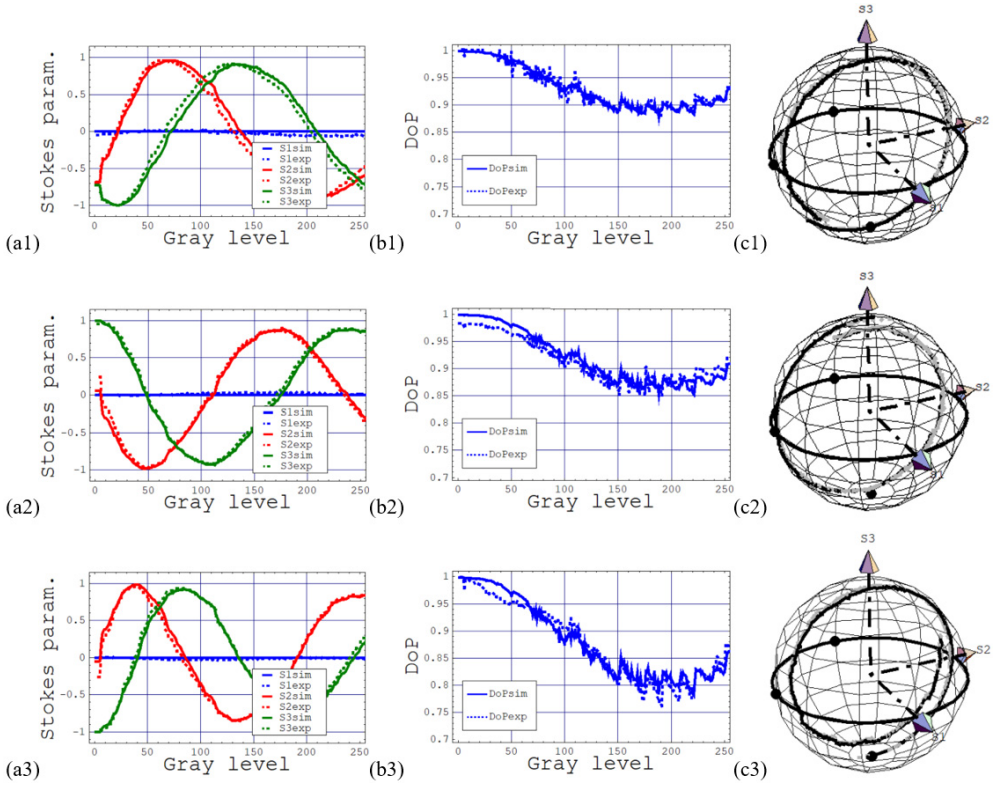

Fig. 7. For sequence format 18-6 and for incident SOP right-handed circular, in plots (a) for the Stokes parameters and in (b) for DoP, experiment (dots) and theoretical prediction with the proposed model (line), and in plots (c) representation on the Poincaré sphere, where the dark line is simulation and gray line is experiment. Top row ((a1), (b1) and (c1)) for 633 nm and incidence at 3°; middle row ((a2), (b2) and (c2)) for 532 nm and incidence at 30°; bottom row ((a3), (b3) and (c3)) for 473 nm and incidence at 30°.

Both in Figs. 6 and 7, the different rows demonstrated that we can use the model to find at which angles of incidences and wavelengths we might obtain a reflected SOP describing a full meridian across the Poincaré sphere. Now in Fig. 8 we want to show the maximum range of SOP modulation that is possible with our current PA-LCoS and for sequence 18-6, which

Optics EXPRESS

produces larger values of depolarized light when compared with sequence 5-5. When using the shorter wavelength, 473 nm, and with light incident perpendicularly to the entrance face of the PA-LCoS is when we obtain the larger modulation range. In the Stokes parameters plot (Fig. 8(a)) we see that there are more oscillations when compared with plots in Figs. 6 and 7. In Fig. 8(b), DoP reaches such a low value as 0.7. In Fig. 8(b), on the Poincaré sphere we see that the curve is describing almost two meridians, with the second turn getting into the inner volume of the Poincaré sphere due to the low values in the DoP.

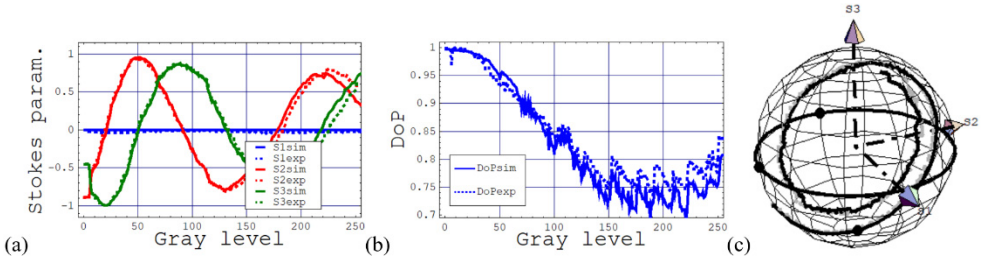

Fig. 8. For sequence format 18-6 and for incident SOP right-handed circular, for 473 nm and at 3° incidence, in plots (a) for the Stokes parameters and in (b) for DoP, experiment (dots) and theoretical prediction with the proposed model (line), and in plots (c) representation on the Poincaré sphere, where the dark line is simulation and gray line is experiment.

Agreement between experiment and model is once again very good, thus showing the accuracy and usefulness of the model in order to design appropriate working configurations (incidence angles, illumination wavelengths, gray level ranges, appropriate input SOP) adapted to the specific application in mind. Next we show some of such applications. In Fig. 9 we are interested in the analysis of the spectral dependence of the SOP and the DoP. We restrict our attention to sequence 5-5, which shows smaller flicker and thus it is the most probable candidate in most of applications.

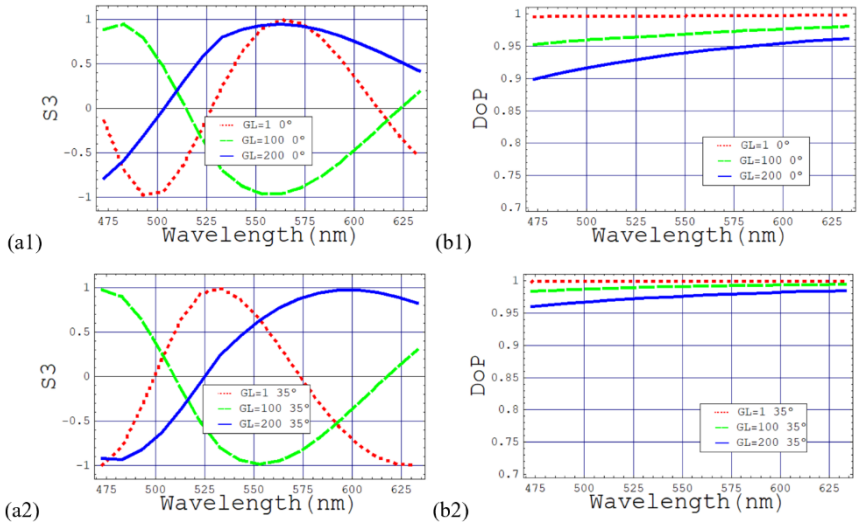

Fig. 9. For sequence format 5-5 and for incident SOP right-handed circular. Simulations for the spectral variation of the Stokes parameter S3 ((a1) and (a2)) and the DoP ((b1) and (b2)), for incidences at 0° ((a1) and (b1)) and at 35° ((a2) and (b2)).

In the first column in Fig. 9, we plot the Stokes parameter S3 as a function of the wavelength across the whole visible range, and in the second column we show the DoP. The results are for three different gray levels, shown in the legend. In the first and second rows the results are respectively for perpendicular incidence and at an angle of 35°. We see that at

Optics EXPRESS

certain gray levels and angles of incidence we have slowest variations in S3, which might be interesting to decrease wavelength dependence when using non-monochromatic sources: in the cases shown chromatic dispersion is smaller at gray level 200. We also show that the DoP magnitude decreases at shorter wavelengths.

An alternative analysis interesting in some applications is the dependence of the reflected SOP from the LCoS when the incident wavefront is not a collimated wavefront. To such cases, in Fig. 10 we show for three gray levels (in the legend) the Stokes parameter S3 (first column) and the DoP (second column) as a function of the angle of incidence. In the first row we plot the curves for the wavelength 633 nm, and for 473 nm in the second row. As in Fig. 9, we restrict our attention to sequence 5-5. We note that in the case of DoP, values for angles larger than 35° might not agree fully with experimental measurements, as commented in previous sections. We see that for example at gray level 100 both for the wavelengths 633 and 473 nm, angular dependence for S3 is very small. We also see for the three gray levels considered, that the S3 parameter changes very little for an angular range of about 10° at perpendicular incidence. In the case of DoP, we have a quantification of its increase as the angle of incidence increases. This is then one strategy to minimize its effects on applications.

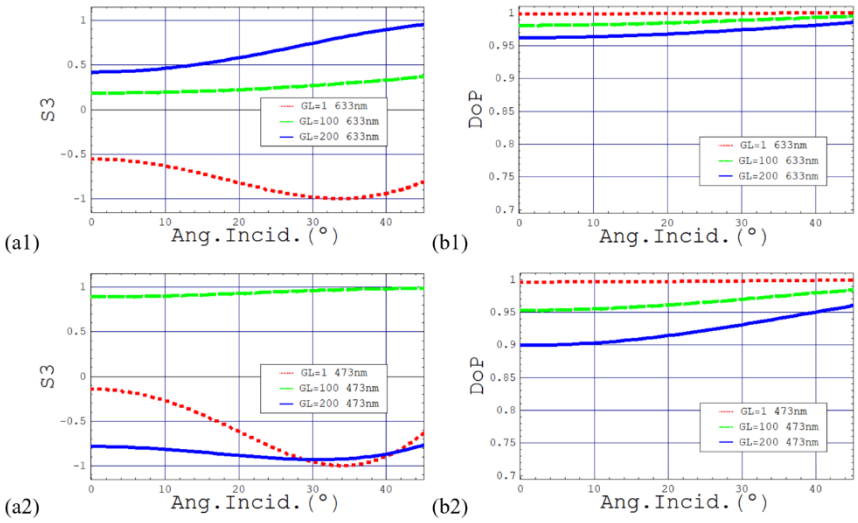

Fig. 10. For sequence format 5-5 and for incident SOP right-handed circular. Simulations for the variation as a function of the angle of incidence for the Stokes parameter S3 ((a1) and (a2)) and for the DoP ((b1) and (b2)), at illumination wavelengths 633 nm ((a1) and (b1)) and 473 nm ((a2) and (b2)).

4. Conclusions

We have demonstrated a very unique model for PA-LC devices, which is able to predict with a high accuracy a wide range of results both without and with flicker included. We have seen that the model describes the angular and wavelength dependencies for retardance, reflected SOP and DoP. For the calibration performed in the paper, the wavelength range comprises the whole visible spectrum. In the case of the incidence angle, the range covered is 0°-45° for the average values and 0°-35° for the flicker amplitudes, which is still a very remarkable range. Prediction of the modulation capabilities and its associated flicker relies on the fitting of the equivalent tilt angle of the molecules as a function of applied voltage, from what we also obtain the amplitude in the flicker of the tilt angle at every applied voltage. Specific results are given for liquid crystal on silicon (PA-LCoS) microdisplays, central to many spatial light modulation applications such as the generation and detection of structured polarized beams. We believe that our approach offers novel capabilities in the generation of arbitrary states of polarization, both fully and partially polarized, since the approach enables to calculate the

Optics EXPRESS

interplay between angle of incidence and illumination wavelength in order to obtain the necessary modulation range for the application in mind. Additionally, calculation of flicker in the tilt angle might be a useful tool to inspect the dynamics of internal properties of LC devices.

Funding

Ministerio de Economía, Industria y Competitividad (Spain) (MINECO/AEI/FEDER, UE) (FIS2017-82919-R); Ministerio de Economía, Industria y Competitividad (Spain) (MINECO/FEDER) (FIS2015-66570-P); Generalitat Valenciana (Spain) (PROMETEO II/2015/015); Universidad de Alicante (Spain) (GRE17-06).

References

1. S.-T. Wu and D.-K. Yang, *Reflective Liquid Crystal Displays* (Wiley, 2001).
2. V. G. Chigrinov, *Liquid Crystal Devices: Physics and Applications* (Artech House, 1999).
3. P. Yeh and C. Gu, *Optics of Liquid Crystal Displays* (Wiley, 2010).
4. N. Collings, T. Davey, J. Christmas, D. Chu, and B. Crossland, "The Applications and Technology of Phase-Only Liquid Crystal on Silicon Devices," J. Disp. Technol. **7**(3), 112–119 (2011).
5. Z. Zhang, Z. You, and D. Chu, "Fundamentals of phase-only liquid crystal on silicon (LCOS) devices," Light Sci. Appl. **3**(10), 213 (2014).
6. J. Turunen and F. Wyrowski, eds., *Diffractive Optics for Industrial and Commercial Applications*, 1. ed. (Akademie Verlag, 1997).
7. H. Coufal, D. Psaltis, and G. T. Sincerbox, eds., *Holographic Data Storage* (Springer, 2000).
8. K. Curtis, L. Dhar, A. Hill, W. Wilson, and M. Ayres, eds., *Holographic Data Storage : From Theory to Practical Systems.* (John Wiley & Sons, 2010).
9. W. Osten, C. Kohler, and J. Liesener, "Evaluation and application of spatial light modulators for optical metrology," Opt. Pura Apl. **38**, 71–81 (2005).
10. M. A. F. Roelens, S. Frisken, J. A. Bolger, D. Abakoumov, G. Baxter, S. Poole, and B. J. Eggleton, "Dispersion Trimming in a Reconfigurable Wavelength Selective Switch," J. Lit. Technol. **26**(1), 73–78 (2008).
11. A. Boutin, C. Koebele, D. Sperti, F. Verluise, G. Charlet, H. Mardoyan, L. Provost, M. Bigot-Astruc, M. Salsi, P. Tran, P. Brindel, P. Sillard, and S. Bigo, "Mode-Division Multiplexing of 2 × 100 Gb/s Channels Using an LCOS-Based Spatial Modulator," J. Lit. Technol. **30**, 618–623 (2012).
12. A. Dudley, G. Milione, R. R. Alfano, and A. Forbes, "All-digital wavefront sensing for structured light beams," Opt. Express **22**(11), 14031–14040 (2014).
13. A. Farré, M. Shayegan, C. López-Quesada, G. A. Blab, M. Montes-Usategui, N. R. Forde, and E. Martín-Badosa, "Positional stability of holographic optical traps," Opt. Express **19**(22), 21370–21384 (2011).
14. M. A. Solís-Prosser, A. Arias, J. J. M. Varga, L. Rebón, S. Ledesma, C. Iemmi, and L. Neves, "Preparing arbitrary pure states of spatial qudits with a single phase-only spatial light modulator," Opt. Lett. **38**(22), 4762–4765 (2013).
15. T. Brown and Q. Zhan, "Introduction: Unconventional Polarization States of Light Focus Issue," Opt. Express **18**(10), 10775–10776 (2010).
16. I. Moreno, J. A. Davis, K. Badham, M. M. Sánchez-López, J. E. Holland, and D. M. Cottrell, "Vector Beam Polarization State Spectrum Analyzer," Sci. Rep. **7**(1), 2216 (2017).
17. X. Zheng, A. Lizana, A. Peinado, C. Ramirez, J. L. Martinez, A. Marquez, I. Moreno, and J. Campos, "Compact LCOS–SLM Based Polarization Pattern Beam Generator," J. Lit. Technol. **33**(10), 2047–2055 (2015).
18. A. Cofré, A. Vargas, F. A. Torres-Ruiz, J. Campos, A. Lizana, M. M. Sánchez-López, and I. Moreno, "Dual polarization split lenses," Opt. Express **25**(20), 23773–23783 (2017).
19. A. Hermerschmidt, S. Osten, S. Krüger, and T. Blümel, "Wave front generation using a phase-only modulating liquid-crystal-based micro-display with HDTV resolution," in *Proceedings of SPIE*, G. Cheriaux, C. J. Hooker, and M. Stupka, eds. (International Society for Optics and Photonics, 2007), **Vol. 6584**, p. 65840E.
20. A. Lizana, I. Moreno, A. Márquez, E. Also, C. Iemmi, J. Campos, and M. J. Yzuel, "Influence of the temporal fluctuations phenomena on the ECB LCoS performance," in *Proceedings of SPIE*, K. M. Iftekharuddin and A. A. S. Awwal, eds. (International Society for Optics and Photonics, 2009), **Vol. 7442**, p. 74420G.
21. J. García-Márquez, V. López, A. González-Vega, and E. Noé, "Flicker minimization in an LCoS spatial light modulator," Opt. Express **20**(8), 8431–8441 (2012).
22. F. J. Martínez, A. Márquez, S. Gallego, M. Ortuño, J. Francés, A. Beléndez, and I. Pascual, "Electrical dependencies of optical modulation capabilities in digitally addressed parallel aligned liquid crystal on silicon devices," Opt. Eng. **53**(6), 067104 (2014).
23. F. J. Martínez, A. Márquez, S. Gallego, J. Francés, I. Pascual, and A. Beléndez, "Retardance and flicker modeling and characterization of electro-optic linear retarders by averaged Stokes polarimetry," Opt. Lett. **39**(4), 1011–1014 (2014).
24. C. Ramirez, B. Karakus, A. Lizana, and J. Campos, "Polarimetric method for liquid crystal displays characterization in presence of phase fluctuations," Opt. Express **21**(3), 3182–3192 (2013).

Optics EXPRESS

25. I A. Lizana, I. Moreno, A. Márquez, C. Iemmi, E. Fernández, J. Campos, and M. J. Yzuel, "Time fluctuations of the phase modulation in a liquid crystal on silicon display: characterization and effects in diffractive optics," Opt. Express **16**(21), 16711–16722 (2008).
26. G. Lazarev, A. Hermerschmidt, S. Krüger, and S. Osten, "LCOS Spatial Light Modulators: Trends and Applications," in *Optical Imaging and Metrology: Advanced Technologies*, W. Osten and N. Reingand, eds. (Wiley-VCH Verlag GmbH & Co. KGaA, 2012), pp. 1–29.
27. D. W. Berreman, "Optics in Stratified and Anisotropic Media: 4×4-Matrix Formulation," J. Opt. Soc. Am. **62**(4), 502–510 (1972).
28. P. Yeh, "Extended Jones matrix method," J. Opt. Soc. Am. **72**(4), 507–513 (1982).
29. C. Gu and P. Yeh, "Extended Jones matrix method II," J. Opt. Soc. Am. A **10**(5), 966–973 (1993).
30. A. Lien, "Extended Jones matrix representation for the twisted nematic liquid-crystal display at oblique incidence," Appl. Phys. Lett. **57**(26), 2767–2769 (1990).
31. F. J. Martínez, A. Márquez, S. Gallego, J. Francés, I. Pascual, and A. Beléndez, "Effective angular and wavelength modeling of parallel aligned liquid crystal devices," Opt. Lasers Eng. **74**, 114–121 (2015).
32. A. Márquez, J. Francés, F. J. Martínez, S. Gallego, M. L. Álvarez, E. M. Calzado, I. Pascual, and A. Beléndez, "Computational split-field finite-difference time-domain evaluation of simplified tilt-angle models for parallel-aligned liquid-crystal devices," Opt. Eng. **57**(03), 1 (2018).
33. J. Francés, A. Márquez, F. J. Martínez-Guardiola, S. Bleda, S. Gallego, C. Neipp, I. Pascual, and A. Beléndez, "Simplified physical modeling of parallel-aligned liquid crystal devices at highly non-linear tilt angle profiles," Opt. Express **26**(10), 12723–12741 (2018).
34. A. Lizana, A. Márquez, L. Lobato, Y. Rodange, I. Moreno, C. Iemmi, and J. Campos, "The minimum Euclidean distance principle applied to improve the modulation diffraction efficiency in digitally controlled spatial light modulators," Opt. Express **18**(10), 10581–10593 (2010).
35. F. J. Martínez, A. Márquez, S. Gallego, M. Ortuño, J. Francés, I. Pascual, and A. Beléndez, "Predictive capability of average Stokes polarimetry for simulation of phase multilevel elements onto LCoS devices," Appl. Opt. **54**(6), 1379–1386 (2015).
36. F. J. Martínez, A. Márquez, S. Gallego, M. Ortuño, J. Francés, A. Beléndez, and I. Pascual, "Averaged Stokes polarimetry applied to evaluate retardance and flicker in PA-LCoS devices," Opt. Express **22**(12), 15064–15074 (2014).
37. F. J. Martínez, A. Márquez, S. Gallego, J. Francés, and I. Pascual, "Extended linear polarimeter to measure retardance and flicker: application to liquid crystal on silicon devices in two working geometries," Opt. Eng. **53**(1), 014105 (2014).
38. J. E. Wolfe and R. A. Chipman, "Polarimetric characterization of liquid-crystal-on-silicon panels," Appl. Opt. **45**(8), 1688–1703 (2006).